RSC Advances

ROYAL SOCIETY OF CHEMISTRY

www.rsc.org/advances

RSC Advances

RSCPublishing

ARTICLE

$Ni(OH)_2$ nanosheets grown on 3D graphene framework as an excellent cathode for flexible supercapacitors†

Cite this: DOI: 10.1039/xoxxoooooox

Received ooth January 2012,
Accepted ooth January 2012

DOI: 10.1039/xoxxoooooox

www.rsc.org/

Yufang Ma, Wanjun Chen, Peng Zhang, Feng Teng, Jinyuan Zhou, Xiaojun Pan*, Erqing Xie*,

$Ni(OH)_2$ nanosheets/3D graphene (3DG) frameworks hybrid materials have been prepared by combining chemical vapor deposition (CVD) technology and a facile hydrothermal method. The free-standing $Ni(OH)_2$ nanosheets/3DG composite was investigated as the cathode material for supercapacitor without the need for addition of either binder or metal-based current collector. Consequently, the obtained $Ni(OH)_2$ nanosheets/3DG composite electrode exhibits superior specific capacitance and rate capability to the $Ni(OH)_2$ nanosheets/Ni foam and $Ni(OH)_2$ nanosheets/carbon fiber cloth composite electrodes. This novel structure brings the composite an electrochemical capacitance as high as 2860 F g^{-1} at a current density of 2 A g^{-1}, and maintains 1791 F g^{-1} at 30 A g^{-1}. Moreover, the composite electrode also exhibits a high specific capacitance of 2461 F g^{-1} at a scan rate of 5 mV s^{-1}.

1. Introduction

Electrochemical capacitors, also called supercapacitors, are regarded as a promising candidate for energy storage because of their outstanding characteristics, such as high power density, long cyclic performance and fast recharge capability[1, 2]. During the past years, a significant amount of efforts have been devoted to flexible supercapacitors because of their potential applications, such as wearable, foldable, and rollable electronic devices[3-9].

Due to the fast reversible faradic redox reactions, compared with electrical double-layer capacitors (EDLCs), pseudocapacitors usually present larger energy density than EDLCs[10]. Transition metal oxides and hydroxides are frequently used as electrode materials of pseudocapacitors for their excellent electrochemical properties[11]. Among all the metal oxides and hydroxides, hydrous RuO_2 showed the best performance. However, the high cost and environmental unfriendliness limits the application of RuO_2. Thus, other economic transition metal oxide or hydroxide materials have been explored, such as MnO_2, $Co(OH)_2$, Co_3O_4, V_2O_5, and NiO[12-18]. Recently, $Ni(OH)_2$ with lower cost, lower toxicity and ease of synthesis, has been widely researched due to its high theoretical specific capacitance caused by fast Ni^{2+}/Ni^{3+} redox reaction[19]. $Ni(OH)_2$ can be classified into two types: α- and β-phase[20, 21]. α-$Ni(OH)_2$ is expected to show superior electrochemical performance due to its poorly or turbostratically crystallized structure. To date, many different $Ni(OH)_2$ samples were reported to be synthesized in water using a hydrothermal process or by a coprecipitation method with surfactant[22-26]. However, the $Ni(OH)_2$ prepared by above mention method generally exhibits poor conductivity and powdery form. Thus, the electrodes that consist of the powdery active materials usually show inefficient charge transport and weak mechanical stability, hindering its electrochemical performance[27-29].

To overcome the drawbacks, a flexible electrode with favorable electrical conductivity and mechanical strength is needed. Graphene, as a two-dimensional material with many advantages like large surface area, high electrical conductivity, fine mechanical flexibility, and lightweight, is considered as an ideal matrix for loading pseudocapacitor materials[30, 31]. Extensive researches have been launched in the fabrication of graphene based composite electrodes for supercapacitor applications, which can combine the advantages of both components and may generate special properties by the reinforcement or modification of each other[32-35]. However, most of works on graphene-based composites were incorporating guest transition metal oxide nanoparticles onto 2D graphene sheets[36-38], and those structures usually suffer from serious aggregation, which would cause inferior accessibility of electrolyte ions to active material surface. Besides, the weak contact of graphene sheets also results in poor electrical conductivity. In order to solve the issue mentioned above, the three-dimensional graphene (3DG) networks were constructed by chemical vapor deposition (CVD) methods[39]. The 3DG networks are excellent templates for the preparation of the 3D metal oxide-graphene hybrid composites which can be used as supercapacitor electrodes. The unique 3D porous structure of the graphene network with a large specific surface area allows the rapid access of electrolyte ions to the metal oxide surface[11, 40, 41]. Due to the enlarged specific surface area of 3D structures, the metal oxide layer can become thinner than that on 2D graphene sheets when the same amount of metal oxide is loaded. The thinner metal oxide layer gives a large active surface area and a better accessibility for

the electrolyte, and results in an improvement of electrochemical performances[42].

Herein, a novel $Ni(OH)_2$ nanosheets/3D graphene composite with hierarchically porous structures by a two-step method has been developed. The $Ni(OH)_2$ nanosheets was uniformly grown onto the as-prepared porous 3DG framework by a facile and efficient hydrothermal method[43]. The graphene sheets overlap with each other to afford a 3D conducting network for fast electron transfer between the active materials and the charge collector. The unique 3D hierarchical structure of the $Ni(OH)_2$ nanosheets/3DG composite hybrid electrode, consisting of interconnected pore channels on both micrometer and nanometer length scales, simultaneously optimizes ion and electron transport and contraction between the active material and electrolyte. As a result, the $Ni(OH)_2$ nanosheets/3DG composite hybrid has exhibited advanced pseudocapacitor performance. In addition, the 3DG networks which are lightweight and flexible than other materials such as Ni foam, carbon fiber cloth have excellent flexibility to provide a template for active materials. The total mass of electrodes is only 0.87 mg, which provides a good choose for portable devices. Furthermore, the raw materials for the experiment are easy to get.

2. Experimental

2.1 Materials

All reagents used in this work were obtained guaranteed as analytical-grade and used without further purification and treatment. Nickel nitrate($Ni(NO_3)_2 \cdot 6H_2O$), urea, poly(methyl methacrylate) (PMMA), hydrogen chloride (HCl), sodium dodecyl benzene sulphonate (SDBS) were purchased from SigmaAldrich Co. LLC (USA). Nickel (Ni) foams and carbon fiber cloth were purchased from Changsha Lyrun New Material Co. Ltd., China. And ethanol was analytical-grade without further purification. Deionized water was used throughout the experiments.

2.2 Growth of the 3D Graphene Networks

The 3D graphene was synthesized by a CVD method on Ni foam used as a template. Ni foam was used to catalyze the graphene growth mentioned in our previous work. Briefly, Ni foam was cut into pieces of 1 cm×2 cm and pressed into a thin sheet (~0.2 mm thick), then ultrasonic cleaned in HCl solution, acetone and deionized water respectively. Second, graphene was grown by CVD method with CH_4 as carbon source for 5 min after Ni foam was cleaned in H_2 and Ar gas atmosphere to eliminate a thin surface oxide layer. Third, the Ni foams were corroded in 6M HCl solution at 80 °C. Before this process, the PMMA solution was dropped on the Ni foams and the samples were annealed at 160 °C for 0.5 h to covered with graphene. Finally, the PMMA was removed by acetone and the three-dimensional graphene networks were obtained[44].

2.3 Synthesis of $Ni(OH)_2$ nanosheets/3DG composite

Pure 3DG foam was achieved after etching the Ni away using a 6M HCl aqueous solution. The $Ni(OH)_2$ nanosheets /3DG composite was prepared by a hydrothermal reaction as follows: Typically, 0.24 mmol $Ni(NO_3)_2 \cdot 6H_2O$ and 4.8 mmol urea were dissolved in 100 mL of distilled water. After the mixture was stirred for 10 min, the 3DG infiltrated by SDBS was placed into the reaction flask[45]. When the 3DG was totally wetted, the mixed solution was kept at 90℃ for 12h and then cooled to room temperature. The resulting $Ni(OH)_2$ nanosheets/3DG composite was then washed using deionized water and ethanol several times, and dried at 80℃ in an air oven. As comparisons, the $Ni(OH)_2$ nanosheets were directly prepared on the Ni foam (NF) and carbon fiber cloth (CFC), respectively. As supplementary, the different composites were made at 90℃ for 12, 24, 36, 48 h, respectively, with other conditions unchanged (These sentences have been provided in the Electronic Supplementary Information (ESI)).

The weight of $Ni(OH)_2$ was 0.12 mg, measured with a Sartorius Microbalance (accuracy: 0.01 mg), and the total mass of electrodes was 0.87 mg, which provides a good choose for portable devices. The reaction time and solution concentration are the determination of mass of $Ni(OH)_2$ nanosheets in the electrodes. Though the more time lead to the more load of the active material, a relatively low conductivity appeared, which was proven in ESI.

2.4 Morphology and structure Characterization

The morphologies of the $Ni(OH)_2$ nanosheets/3DG composite were investigated by field emission scanning electron microscope (FE-SEM, Hitachi S-4800) and high resolution transmission electron microscope (HR-TEM, FEI Tecnai F30, operated at 300 kV) equipped with energy dispersive X-ray spectroscopy (EDX, Oxford Instrument, UK). The crystal structure was characterized by X-ray diffraction (XRD, Rigaku, D/max-2400, Cu Kα, 0.154056 nm) with a range of 2θ from 5 to 80° at a rate of 5° min^{-1} and Raman spectroscopy (JY-HR800 micro-Raman, using a 532 nm wavelength YAG laser with a laser spot diameter of about 600 nm). The composition was examined by Fourier transform infrared spectroscopy (FTIR, NEXUS 670) in the range of 400~4000 cm^{-1}.

2.5 Electrochemical Characterization

A three-electrode system was used to measure the response of the $Ni(OH)_2$ nanosheets/3DG composite as the working electrode using 6 M KOH aqueous solution as electrolyte, with a Pt-flake (1 cm × 1 cm) as the counter electrode and Ag/AgCl (in sat. KCl) as the reference electrode, respectively. The mass loading of $Ni(OH)_2$ nanosheets on 3DG network (area of 1 cm by 1 cm) is 0.15 mg/cm^2 . Electrochemical impedance spectroscopy (EIS) measurements, cyclic voltammogram (CV) and galvanostatic charge-discharge (GCD) were performed with an electrochemical workstation (RST5200, Zhengzhou Shiruisi Instrument Technology Co., Ltd, China).

3. Results and discussion

The XRD patterns of original 3D graphene and $Ni(OH)_2$ nanosheets/3DG composite are shown in Figure 1a. It can be seen that two strong peaks at 21.5° and 26.5° were found, indicating the (002) and (004) plane of graphene and the (002) plane has the strongest peak intensity, indicating that the crystallinity of the 3D graphene is fine. It also describes the graphene lattice defects is relatively small. A weak peak at 11.6° can be indexed as relatively low crystallization α-$Ni(OH)_2$ with a flaky structure (JCPDS No.38-0715). From Figure 1b, the containing elements of the composite can be observed clearly. The Raman spectra of $Ni(OH)_2$ nanosheets/3DG composite and the pristine 3DG are shown in Figure 1c. It can be clearly seen that there are three main peaks at 460, 1350 and 3645 cm^{-1} in the composite, which are contributed to the α-$Ni(OH)_2$[46]. Further experiments had been done: 6 M HCl was used to remove the $Ni(OH)_2$ nanosheets on 3DG and achieved the processed 3DG. Raman characterization testing was applied to the processed 3DG. The comparison results are supplied in the figure S4. The Raman spectra of processed 3DG is just lower than the original graphene on the

signal intensity, no obvious D-band (usually at ≈1300 cm^{-1}) means that the $Ni(OH)_2$ introduce few defects to the graphene (ESI). According the above results, we can concluded that after $Ni(OH)_2$ deposition the diffraction intensity of the graphene nanosheets has no obvious attenuation, which imply that the slice of $Ni(OH)_2$ nanosheets are adhering to the 3DG and have few impact of graphene signals. After $Ni(OH)_2$ deposition, the diffraction intensity of the graphene nanosheets has no obvious attenuation, which imply that the slice of $Ni(OH)_2$ nanosheets are adhering to the 3DG and have few impact of graphene signals. FTIR spectra reveal the existence of –OH (~3436.9 cm^{-1}), C≡C (2222.3 cm^{-1}), C=C (1628.1 cm^{-1}), and C–O (1054.1 cm^{-1}) functional groups in composite (Figure 1d). And the small peak at 472.8 cm^{-1} can be assigned to Ni–O vibrations and Ni–O–H bending vibrations that can be ascribed to Ni–OH. The sharp and narrow band at 3641.9 cm^{-1} of α-$Ni(OH)_2$ is attributed to the ν_{O-H} stretching vibration[47].

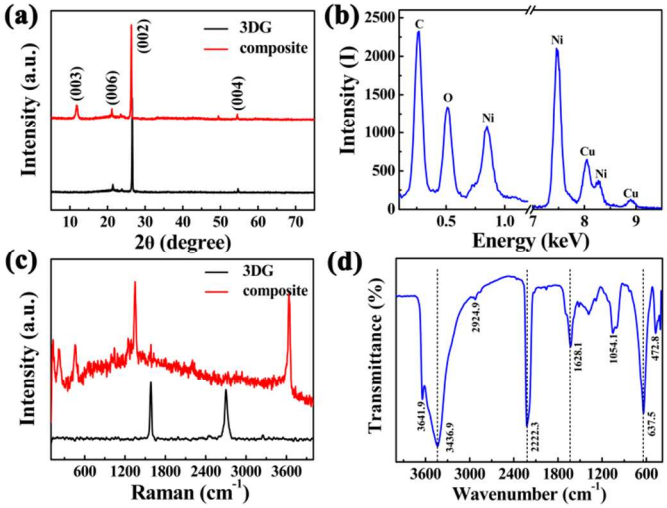

Figure 1. (a) XRD patterns of the $Ni(OH)_2$ nanosheets/3DG composite and the 3DG. (b) EDX pattern of the $Ni(OH)_2$ nanosheets/3DG composite.(c) Raman spectra of the $Ni(OH)_2$ nanosheets/3DG composite and the 3DG.(d) FTIR spectrum of the $Ni(OH)_2$ nanosheets/3DG composite.

The SEM image in Figure 2a shows that the obtained $Ni(OH)_2$ film on the 3DG framework. No collapse of the graphene skeleton is observed, indicating the strong mechanical strength of the 3DG and the light weight of the $Ni(OH)_2$ film (S2a). Acceding our observation, the $Ni(OH)_2$ film is well adhered to the 3D graphene surface (see ESI). The $Ni(OH)_2$ thin film exhibits a highly random porous architecture, which is composed of nanoflakes with tiny thickness (Figure 2b, Figure S3).

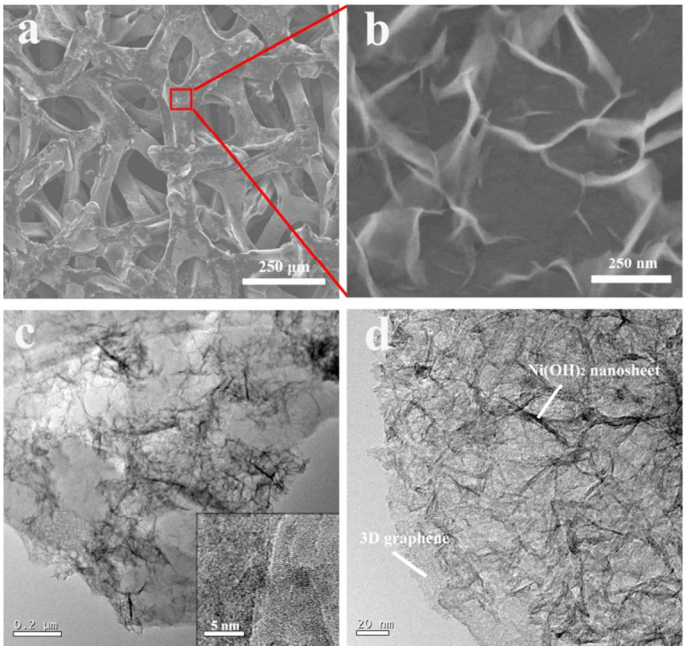

Figure 2. (a) SEM images of the composite. (b) higher magnification of the $Ni(OH)_2$ nanoflakes. (c) TEM image of the composite, and the inset shows a higher magnification of the composite. (d) TEM image showing a flower-like nanostructure composed of nanosheets.

TEM observation is further conducted to probe the microstructure, as shown in Figure 2c, the multilayer structure of $Ni(OH)_2$ nanosheets can be identified in the high resolution TEM images. The $Ni(OH)_2$ sample with low crystallinity consists of random nanosheets (Figure 2c, inset), which agglomerate to form fine-grained microstructure. The typical image (Figure 2d) shows that it has a folding silk-like morphology with transparent features. By introducing graphene substrate, the flower-like $Ni(OH)_2$ are well inherited and decorate homogeneously on the graphene sheets. Here, urea as a mild reducing agent can be mixed with nickel salt heating to form a uniform hybrid of Ni complexes during the preparation of the composite. Therefore, when graphene nanosheets are introduced, the obtained composites can combine the high electrical conductivity of graphene with higher pesudocapacitance of $Ni(OH)_2$ at the same time, and form a 3D hierarchical porous structure. Undoubtedly, such porous building blocks would ensure the good structure stability, cycle stability and rate capability of the active material during the charge and discharge processes.

The electrochemical properties of the porous $Ni(OH)_2$ sample was evaluated initially by cyclic voltammetry (CV, Figure 3a) in the potential range of -0.10 to 0.40 V (vs. silver chloride electrode) at various scan rates. The shape of the CV curves reveal that the capacitance behavior was a result of pseudocapacitor based on redox mechanisms instead of an electric double layer capacitor, whose CV curve appears rectangular in shape. The specific capacitances (SCs) of the $Ni(OH)_2$ nanosheets/3DG composite sample, which corresponded with the results of the CV test, showed a good performance as we expected. The main reactions in the system are as follows:

$$CO(NH_2)_2 + H_2O \leftrightarrow 2NH_3 + CO_2 \quad (1)$$
$$NH_3 + H_2O \leftrightarrow OH^- + (NH_4)^+ \quad (2)$$
$$Ni^{2+} + 2OH^- \leftrightarrow Ni(OH)_2 \quad (3)$$

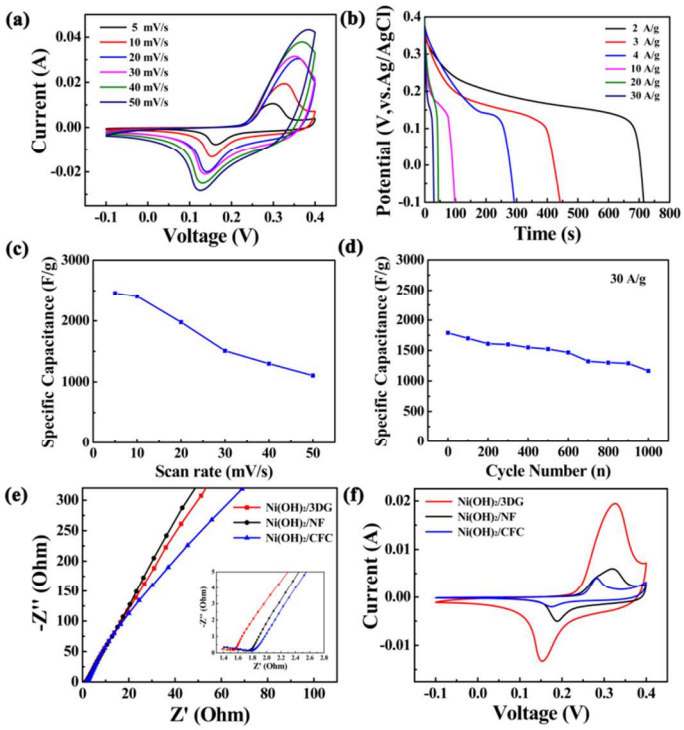

Figure 3. The electrochemical performance of $Ni(OH)_2$ nanosheets/3DG composite: (a) CV curves at various scan rates; (b) galvanostatic charge-discharge curves at different current densities; (c) specific capacitance as a function of the scan rate; (d) cycling performance of the composite at 30 A g^{-1}; (e) Nyquist plots and (f) CV curves at 10 mV s^{-1} of the three comparison samples.

As shown in Figure 3a, a couple of redox peaks is observed between -0.1 V and 0.4 V versus CSE. These peaks correspond to the extraction and insertion of proton and can be represented by the following equation:[47]

$$\alpha\text{-}Ni(OH)_2 + OH^- \leftrightarrow \gamma\text{-}NiOOH + H_2O + e^- \quad (4)$$

These redox peaks still can be observed clearly which are showing no significant change at various scan rates from 5 to 50 mV s^{-1}, indicating the perfect rate performance. It can be observed clearly, with increasing the scan rate, the current increased, the oxidation peaks shifted to a more positive position and the reduction peaks to a more negative position. This is probably due to the diffusion effect of protons within the electrode that parts of the surface of the electrode are inaccessible at high charging-discharging rates[48, 49].

Figure 3b gives the charge-discharge curves of the $Ni(OH)_2$ nanosheets/3DG composite at different currents. The capacitance (C, F) of $Ni(OH)_2$ nanosheets/3DG composite electrode was calculated by the following equation:

$$C = I \times t/\Delta V \quad (5)$$

where I, t and ΔV correspond to the discharge current, discharge time, and potential window for charge/discharge, respectively. It is impressive that the $Ni(OH)_2$/graphene nanosheet provides a large specific capacitance of 2860 F g^{-1} at a low current density of 2 A g^{-1}. The specific capacitance (1791 F g^{-1}) still remains even at a large current density of 30 A g^{-1}. These results suggest that the composite electrode have an ideal capacitor performance.

The specific capacitance was calculated from CV curves according to the following equation:

$$C = (\int I \times dV)/(v \times m \times \Delta V) \quad (6)$$

where I is the voltammetric current as a function of potential (V) applied on electrode, m is the mass of $Ni(OH)_2$ film, v is the potential scan rate. The specific capacitances are calculated to be 2461, 2402, 1976, 1507, 1297 and 1104 F g^{-1} at the scan rates of 5, 10, 20, 30, 40 and 50 mV s^{-1}, respectively. The specific capacitance decreased gradually with the increased current rate (Figure 3c). It is noticeable that a high specific capacitance of 1104 F g^{-1} with a retention capacitance of about 49% can still be preserved, when the scan rate is increased from 5 mV/s to 50 mV/s.

The long cycle stability of the active materials is critical to the performance of supercapacitors. The cycle test was carried out to examine the electrochemical stability of the as-prepared electrode at a current density of 30 A g^{-1}, as shown in Figure 3d. It is noted that after 1000 cycles, the capacitance retention of the $Ni(OH)_2$ nanosheets/3DG composite is 65%.

EIS was recorded under the following conditions alternating current (AC) voltage amplitude of 5 mV, frequency range of 100 kHz to 0.1 Hz, and open circuit potential. The Nyquist plots of the $Ni(OH)_2$ nanosheets/3DG composite electrode have an almost vertical line in the low frequency region, indicating a good capacitive behavior. Figure 3e illustrates that though $Ni(OH)_2$ nanosheets/3DG composite has relatively poorer electrical conductivity than the $Ni(OH)_2$ nanosheets/NF composite, it's because that electroconductivity is superior to the $Ni(OH)_2$ nanosheets/CFC composite.

Moreover, the capacitance of the $Ni(OH)_2$ nanosheets/3DG composite is larger than that of the two kinds of composites who are $Ni(OH)_2$ nanosheets/NF and $Ni(OH)_2$ nanosheets/CFC composite obviously in Figure 3f. The good rate capability is mainly attributed to the unique 3D hierarchical porous structure and the improved conductivity in the composite.

Conclusions

In summary, a simple and scalable hydrothermal method is used to fabricate the $Ni(OH)_2$ nanosheets/3D graphene composite. The composite present a simple fabrication method for a 3D hierarchical porous structure of $Ni(OH)_2$ nanosheets as building blocks, which is assembled tightly on the matrix of the 3D graphene. Correspondingly, as an active material for supercapacitors in alkaline solution, the $Ni(OH)_2$ nanosheets/3DG composite presents high specific capacitance, good rate capability and long cycle stability, as compared to the $Ni(OH)_2$ nanosheets/NF and the $Ni(OH)_2$ nanosheets/CFC composites. More specifically, the $Ni(OH)_2$ nanosheets/3DG composite exhibits the specific capacitance as high as 2860 F g^{-1} at the current density of 2 A g^{-1}, and is able to endure the high discharge rate at the current density of 30 A g^{-1}, showing excellent rate capability. Such improvement in the performance of the composite is considered in the fabrication of the unique 3D hierarchical porous structure of $Ni(OH)_2$ nanocrystals as building blocks on the matrix of frameworks like 3DG et cetera.

Acknowledgements

We acknowledge the financial support by the National Natural Science Foundation of China (No. 61176058 and No. U1232121) and the National Science Foundation for Post-doctoral Scientists of China (No. 2012M512046).

Notes and references

[a] School of physical science and technology, Lanzhou University, Lanzhou 730000, China
*Corresponding authors. E-mail: xjpan@lzu.edu.cn (X. J. Pan); xieeq@lzu.edu.cn (E. Q. Xie). Fax: +86-931-8913554; Tel: +86-931-8912616.

† Electronic Supplementary Information (ESI) available: [Different composites were made at 90℃ for 12, 24, 36, 48 h, respectively, with other conditions unchanged]. See DOI: 10.1039/b000000x/

1 L. L. Zhang, R. Zhou and X. S. Zhao, *J. Mater. Chem.*, 2010, **20**, 5983.
2 Q. Shou, J. Cheng, L. Zhang, B. J. Nelson and X. Zhang, *J. Solid State Chem.*, 2012, **185**, 191.
3 W. Zeng, L. Shu, Q. Li, S. Chen, F. Wang and X.-M. Tao, *Adv. Mater.*, 2014.
4 Y.-Y. Horng, Y.-C. Lu, Y.-K. Hsu, C.-C. Chen, L.-C. Chen and K.-H. Chen, *J. Power Sources*, 2010, **195**, 4418.
5 C. Meng, C. Liu, L. Chen, C. Hu and S. Fan, *Nano Lett.*, 2010, **10**, 4025.
6 J. Ge, G. Cheng and L. Chen, *Nanoscale*, 2011, **3**, 3084.
7 Y. J. Kang, H. Chung, C.-H. Han and W. Kim, *Nanotechnology*, 2012, **23**, 065401.
8 P. Tang, L. Han and L. Zhang, *ACS Appl. Mater. Interfaces*, 2014, **6**, 10506.
9 Y. He, W. Chen, C. Gao, J. Zhou, X. Li and E. Xie, *Nanoscale*, 2013, **5**, 8799.
10 Q. Li, F. Liu, L. Zhang, B. J. Nelson, S. Zhang, C. Ma, X. Tao, J. Cheng and X. Zhang, *J. Power Sources*, 2012, **207**, 199.
11 T. Chen, Y. Xue, A. K. Roy and L. Dai, *ACS Nano*, 2014, **8**, 1039.
12 X. Xie, C. Zhang, M.-B. Wu, Y. Tao, W. Lv and Q.-H. Yang, *Chem. Commun.*, 2013, **49**, 11092.
13 F. Cao, G. X. Pan, X. H. Xia, P. S. Tang and H. F. Chen, *J. Power Sources*, 2014, **264**, 161.
14 L. Shen, Q. Che, H. Li and X. Zhang, *Adv. Funct. Mater.*, 2014, **24**, 2360.
15 B. Vidhyadharan, N. K. M. Zain, I. I. Misnon, R. A. Aziz, J. Ismail, M. M. Yusoff and R. Jose, *J. Alloys Compd.*, 2014, **610**, 143.
16 S. X. Wang, C. C. Jin and W. J. Qian, *J. Alloys Compd.*, 2014, **615**, 12.
17 Z. Wang, J. Zhu, P. Sun, P. Zhang, Z. Zeng, S. Liang and X. Zhu, *J. Alloys Compd.*, 2014, **598**, 166.
18 X. Xu, J. Shen, N. Li and M. Ye, *J. Alloys Compd.*, 2014, **616**, 58.
19 H. Wang, H. S. Casalongue, Y. Liang and H. Dai, *J. Am. Chem. Soc.*, 2010, **132**, 7472.
20 J. Huang, P. Xu, D. Cao, X. Zhou, S. Yang, Y. Li and G. Wang, *J. Power Sources*, 2014, **246**, 371.
21 J. T. Zhang, S. Liu, G. L. Pan, G. R. Li and X. P. Gao, *J. Mater. Chem. A*, 2014, **2**, 1524.
22 G.-W. Yang, C.-L. Xu and H.-L. Li, *Chem. Commun.*, 2008, 6537.
23 J. Li, W. Zhao, F. Huang, A. Manivannan and N. Wu, *Nanoscale*, 2011, **3**, 5103.
24 X. a. Chen, X. Chen, F. Zhang, Z. Yang and S. Huang, *J. Power Sources*, 2013, **243**, 555.
25 X. Wang, Y. Wang, C. Zhao, Y. Zhao, B. Yan and W. Zheng, *New J. Chem.*, 2012, **36**, 1902.
26 X. Wang, J. Liu, Y. Wang, C. Zhao and W. Zheng, *Mater. Res. Bull.*, 2014, **52**, 89.
27 L. Wang, H. Chen, F. Cai and M. Chen, *Mater. Lett.*, 2014, **115**, 168.
28 M. Li, S. Xu, Y. Zhu, P. Yang, L. Wang and P. K. Chu, *J. Alloys Compd.*, 2014, **589**, 364.
29 W. Hong, J. Wang, L. Niu, J. Sun, P. Gong and S. Yang, *J. Alloys Compd.*, 2014, **608**, 297.
30 Y. Zhu, S. Murali, W. Cai, X. Li, J. W. Suk, J. R. Potts and R. S. Ruoff, *Adv. Mater.*, 2010, **22**, 3906.
31 W. Zhang, C. Ma, J. Fang, J. Cheng, X. Zhang, S. Dong and L. Zhang, *RSC Adv.*, 2013, **3**, 2483.
32 B. G. Choi, S.-J. Chang, H.-W. Kang, C. P. Park, H. J. Kim, W. H. Hong, S. Lee and Y. S. Huh, *Nanoscale*, 2012, **4**, 4983.
33 Y. Meng, K. Wang, Y. Zhang and Z. Wei, *Adv. Mater.*, 2013, **25**, 6985.
34 L. Peng, X. Peng, B. Liu, C. Wu, Y. Xie and G. Yu, *Nano Lett.*, 2013, **13**, 2151.
35 F. Zhang, Y. Lu, X. Yang, L. Zhang, T. Zhang, K. Leng, Y. Wu, Y. Huang, Y. Ma and Y. Chen, *Small*, 2014, **10**, 2285.
36 J. W. Lee, A. S. Hall, J.-D. Kim and T. E. Mallouk, *Chem. Mater.*, 2012, **24**, 1158.
37 D. Yu and L. Dai, *J. Phy. Chem. Lett.*, 2009, **1**, 467.
38 Q. Du, M. Zheng, L. Zhang, Y. Wang, J. Chen, L. Xue, W. Dai, G. Ji and J. Cao, *Electrochim. Acta*, 2010, **55**, 3897.
39 X. Cao, Y. Shi, W. Shi, G. Lu, X. Huang, Q. Yan, Q. Zhang and H. Zhang, *Small*, 2011, **7**, 3163.
40 L. Gao, G.-X. Ni, Y. Liu, B. Liu, A. H. C. Neto and K. P. Loh, *Nature*, 2013, **505**, 190.
41 N. Jung, S. Kwon, D. Lee, D. M. Yoon, Y. M. Park, A. Benayad, J. Y. Choi and J. S. Park, *Adv. Mater.*, 2013, **25**, 6854.
42 X. Huang, Z. Yin, S. Wu, X. Qi, Q. He, Q. Zhang, Q. Yan, F. Boey and H. Zhang, *Small*, 2011, **7**, 1876.
43 J. Ji, L. L. Zhang, H. Ji, Y. Li, X. Zhao, X. Bai, X. Fan, F. Zhang and R. S. Ruoff, *ACS Nano*, 2013, **7**, 6237.
44 W. Chen, Y. He, X. Li, J. Zhou, Z. Zhang, C. Zhao, C. Gong, S. Li, X. Pan and E. Xie, *Nanoscale*, 2013, **5**, 11733.
45 B. Cheng, Y. Le, W. Cai and J. Yu, *J. Hazard. Mater.*, 2011, **185**, 889.
46 J. Yan, Z. Fan, W. Sun, G. Ning, T. Wei, Q. Zhang, R. Zhang, L. Zhi and F. Wei, *Adv. Funct. Mater.*, 2012, **22**, 2632.
47 S. Yang, X. Wu, C. Chen, H. Dong, W. Hu and X. Wang, *Chem. Commun.*, 2012, **48**, 2773.
48 U. M. Patil, K. V. Gurav, V. J. Fulari, C. D. Lokhande and O. S. Joo, *J. Power Sources*, 2009, **188**, 338.
49 Q. D. Wu, X. P. Gao, G. R. Li, G. L. Pan, T. Y. Yan and H. Y. Zhu, *J. Phys. Chem. C*, 2007, **111**, 17082.